ACS OMEGA

http://pubs.acs.org/journal/acsodf

Article

Effect of Support on Stability and Coke Resistance of Ni-Based Catalyst in Combined Steam and CO_2 Reforming of CH_4

Phan Hong Phuong, Ha Cam Anh, Nguyen Tri, Nguyen Phung Anh, and Luu Cam Loc*

Cite This: *ACS Omega* 2022, 7, 20092−20103

Read Online

ACCESS | Metrics & More | Article Recommendations | Supporting Information

ABSTRACT: Ni-based catalysts dispersed on different supports (MgO-α-Al_2O_3, CeO_2, SBA-15, and MgO-SBA-15) were prepared by the impregnation method. Characteristics of the catalysts, including specific surface areas (N_2 physisorption), crystalline phase compositions (powder X-ray diffraction, Raman spectroscopy), reducibility (hydrogen temperature-programmed reduction, H_2-TPR), and morphology (scanning electron microscopy (SEM) and transmission electron microscopy, TEM)) were investigated. The activity and stability of the catalysts were tested for the combined steam and CO_2 reforming of methane at 700 °C in a microflow system. The results show that the catalysts exhibit high activity in the BRM reaction. At 700 °C, the conversion of CH_4 and CO_2 reached 86−99% and 67−80%, respectively, in which the Ni/Mg−SBA catalyst is the best with conversions of CH_4 and CO_2 reaching 99% and 80%. Coke accumulation on the surface of the catalysts for 100 h time on stream (TOS) was evaluated by the temperature-programmed oxidation (TPO) technique. The major cause of the catalytic deactivation was elucidated by combining the determination of the amount and type of deposited coke with the changes in the physicochemical properties of the catalysts after the long-term reaction. Almost complete loss of activity was observed on Ni/Mg−Al catalyst after 100 h TOS, while the activity drop was slow on the Ni/Mg−SBA sample, about 15−20% of the total value. Otherwise, the Ni/CeO_2 and Ni/SBA catalysts firmly retained their stable activity for 100 h TOS due to the minimal carbon deposition and stability of these catalysts' structure. The highly considerable formation of inert C_γ carbon and sintering over Ni catalyst supported on MgO-α-Al_2O_3 were responsible for the lower stability of this catalyst compared to those supported on CeO_2 and SBA-15.

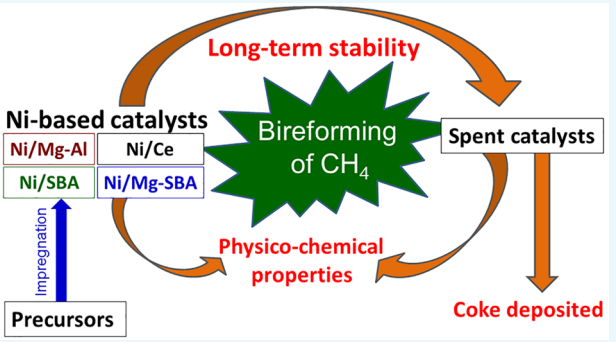

1. INTRODUCTION

The combination of steam reforming (eq 1) and CO_2 reforming (eq 2) of CH_4 in bireforming (eq 3) has been particularly interesting because, on one hand, it converts the two main greenhouse gases (GHG) CO_2 and CH_4 to hydrogen (H_2) and syngas and, on the other hand, has a lower reaction heat (+220 vs +247.3 kJ/mol) than dry methane reforming (DRM).

$$CH_4 + H_2O \rightleftharpoons CO + 3H_2 \quad \Delta H_{298} = +206.3\ \text{kJ/mol} \tag{1}$$

$$CH_4 + CO_2 \rightleftharpoons 2CO + 2H_2 \quad \Delta H_{298} = +247.3\ \text{kJ/mol} \tag{2}$$

$$3CH_4 + CO_2 + 2H_2O \rightleftharpoons 4CO + 8H_2 \quad \Delta H_{298} = +220\ \text{kJ/mol} \tag{3}$$

However, the problem with catalyst deactivation by coke accumulation via the Boudouard reaction, CH_4 decomposition,[1] and metal sintering due to the catalysts' poor thermal stability under a high processing temperature has limited the commercial application of methane reforming. To overcome these disadvantages of Ni-based catalysts in CH_4 reforming, changing the support and/or adding a promoter to modify the physicochemical properties of the catalysts could be applied.[2]

Among the methods, changing the support seems to be a simple and efficient way to prevent catalysts from deactivation by coke formation and Ni sintering. It has been shown in numerous publications that the support acidity[3] and the dimensions of the catalytically active components strongly influenced carbon deposition.[4] Wang et al.[5] stated that the Ni/La_2O_3, Ni/α-Al_2O_3, Ni/SiO_2, and Ni/CeO_2 catalysts exhibited very high activity and moderate deactivation, while the Ni/MgO and Ni/TiO_2 samples had lower activity and better stability. The amount of coke formed after the dry reforming of methane depended strongly on the nature of the support and decreased in the following order Ni/La_2O_3 > Ni/α-Al_2O_3 >

Received: March 29, 2022
Accepted: May 24, 2022
Published: June 2, 2022

Ni/SiO_2 > Ni/MgO > Ni/CeO_2 at 700 °C. Al_2O_3 is usually utilized as a support for Ni-based catalysts during reforming reactions. However, several issues such as carbon deposition, loss of active phase, and formation of inactive spinel phase such as nickel aluminate ($NiAl_2O_4$) leading to catalyst deactivation need to be overcome.[6] Recently, the mesoporous support SBA-15, which has a well-ordered, two-dimensional hexagonal porous network, thick pore walls (3.1−6.4 nm), and thermostability, has been of interest to be used as a support for Ni catalysts in methane reforming.[7] The uniform mesoporous channels of SBA-15 can anchor the metal particles inside the pores, conduct a confinement effect, and restrict their mobility. As a result, the sintering resistance of the catalyst at high temperature would be improved.[8] Furthermore, SBA-15 is a material with a large specific surface area, large pore size, and strong metal to support interaction, supplying a high dispersion of the active metal on the surface, which give good catalytic activity and stability.[9]

Ceria (CeO_2) is considered to be an "active support" which is able to improve the dispersion of the active metal[10] and enhance the performance of transition metals through strong metal−support interactions.[11] Furthermore, CeO_2 is known to be a material with high oxygen storage; its redox properties ($Ce^{4+} \leftrightarrow Ce^{3+}$) promote the formation of oxygen vacancies, thus enhancing the mobility of surface oxygen.[12] Besides, the reduced CeO_{2-x} species accelerates the transfer of activated oxygen from H_2O and CO_2 to the catalyst surface on which the coke is gasified into CO and CO_2.[13]

The activity and stability of nickel catalysts in methane reforming can be further enhanced by modifying the support with other active metal oxides. There have been several studies showing that a basic catalyst could decrease coke formation by promoting the reaction between coke formed and CO_2 in the feed.[14] Introducing basic alkaline or earth alkaline oxides such as K, Mg, Ba, or Ca as promoters for the Ni catalyst can reduce the acidic sites of the catalyst and favor the adsorption of CO_2 species.[15] The promoter MgO is able to enhance the basicity and Ni dispersion of Ni catalysts via a metal−support interaction.[16] The strong basicity of Mg is able to increase CO_2 adsorption that eliminates carbonaceous species such as CH_x at the catalyst surface, enhances carbon gasification,[15] and avoids CO disproportionation, thus improving coke resistance[17] and catalyst stability.[18] The high activity and stability of Mg-modified Ni/Al_2O_3 catalysts are due to the beneficial effects of MgO such as enhancement of steam adsorption, basic property, nanosized NiO crystallite, and strong interaction between Ni and the support.[19]

In our previous studies, NiO catalysts supported on various supports such as α-Al_2O_3 promoted by MgO,[20] CeO_2 of different morphologies,[21] mesoporous nanosilica SBA-15,[22] and MgO-promoted SBA-15[23] have been prepared and investigated for dry and bireforming of methane. The results show that the superior activity of NiO supported on CeO_2-nanorods (CeO_2-NR) has been attributed to the stronger interaction of NiO with CeO_2-NR. In addition, the optimal composition of the catalyst and the most favorable calcination and reduction conditions for catalyst synthesis in the reforming reaction have been determined. The optimal compositions of the catalysts were determined to be as follows: 5.2 wt % Ni/(8.0 wt % Mg + α-Al_2O_3), 7.8 wt % Ni/CeO_2-NR, 31.2 wt % Ni/SBA-15, and 31.2 wt % Ni/(9 wt %Mg + SBA-15). Among these samples, the most suitable calcination temperature is 900 °C for the first catalyst and 800 °C for the remaining catalysts. It was indicated that these catalysts exhibited high performance in DRM and BRM. The optimal composition and calcination conditions determined in those studies will be applied in the synthesis of the catalysts in this study. However, in these investigations, the stability of the catalysts and the cause of catalyst deactivation have not been surveyed. Catalyst stability and deactivation are important properties of the catalysts, and without a thorough understanding of these issues, commercial catalysts cannot be fabricated.

On the basis of the results obtained in the prior publication,[23] in this report, long-term stability tests of Ni catalysts supported on CeO_2, SBA-15, MgO-α-Al_2O_3, and MgO-SBA-15 in the BRM reaction have been conducted. The carbon deposited and the changes of the catalyst's characteristics during the reaction have been investigated. In addition, through the combination and comparison, the relationships between the catalysts' composition, properties, activity, stability, and coke deposition will be elucidated. Consequently, the influence of coke and the carrier on the properties of the nickel catalyst system for the BRM reaction will be clarified.

2. EXPERIMENTAL SECTION

Catalyst Preparation. The catalysts with the optimal composition were prepared using the procedures in previous studies.[20−22] The nonmodified catalysts, i.e., 7.8 wt % Ni supported on CeO_2-NR (Ni/CeO_2) and 31.2 wt % Ni on SBA-15 (Ni/SBA), were prepared by the impregnation method according to the procedure described in detail in refs 21 and 22. The catalysts supported on Mg-modified carriers, including 5.2 wt % Ni and 8.0 wt % Mg on α-Al_2O_3 (Ni/Mg−Al) and 31.2 wt % Ni and 9.0 wt % Mg on SBA-15 (Ni/Mg−SBA), were synthesized by the coimpregnation method of $Ni(NO_3)_2$ and $Mg(NO_3)_2$ solutions onto the corresponding supports. After vaporization and drying, the catalysts were calcined in an air stream at 900 °C for 3 h for the Ni/Mg−Al catalyst, 800 °C for 2 h for Ni/Ce, and 800 °C for 0.5 h for two SBA-15-supported catalysts.

Catalyst Characterization. The crystalline structures of the prepared catalysts were investigated by X-ray diffraction (XRD) using a Bruker D2 Phaser powder diffractometer with Cu Kα radiation (λ = 0.15406 nm) varying 2θ in the range of 10−80°. The Raman spectra were obtained at room temperature with a laser Raman spectrometer (Invia, Renishaw, UK). The hydrogen temperature-programmed reduction (H_2-TPR) was carried out in a gas mixture of 10% H_2/N_2 at a flow rate of 30 mL/min, and the temperature was raised from room temperature to 900 °C with a heating rate of 10 °C/min. The morphology of the catalysts and the particle size of the active phase were characterized by scanning electron microscopy (SEM) and transmission electron microscopy (TEM).

Catalyst Performance Evaluation. Before reaction, the catalyst was reduced in situ in pure H_2 (3 L/h) for 2 h at 800 °C. The activity for BRM of the prepared catalysts was tested in a microflow reactor under atmospheric pressure at 700 °C, and the molar ratio of $CH_4/CO_2/H_2O$ in the feed was 3:1.2:2.4 as detailed in a previous report.[24] Steam was supplied as a saturated vapor in the N_2 gas stream. The catalyst stability over 100 h TOS in the BRM reaction was carried out under similar conditions with a feed flow rate of 15 L/h and catalyst mass of 0.5 g. The reaction mixture was analyzed on an Agilent 6890 Plus Gas Chromatograph (HP-USA) using both a TCD detector (capillary column HP-PLOT Molesieve 5A) and a FID detector (capillary column DB624). The amount of coke

https://doi.org/10.1021/acsomega.2c01931
ACS Omega 2022, 7, 20092−20103

Table 1. Textural Properties of the As-Prepared Catalysts

catalysts	S_{BET}[a] (m^2/g)	d_{por}[a] (nm)	V_{por}[a] (cm^3/g)	d_{cry}[b] (nm)	d_{NiO}[c] (nm)	T_{max}[d] (°C)	m_{Ni^0}[d] (mmol/g)	m_{CO_2}[e] (au)
Ni/Mg−Al[20]	7.1	2.02	0.002	25.6 (Al_2O_3)	20−30	337; 875	0.124	3.69
Ni/CeO_2[21]	46.8	2.15	0.023	23.7 (CeO_2)	2−5; 10−20	250; 330; 352; 395; 816	0.266	9.83
Ni/SBA[22]	232.6	6.08	0.291	18.4 (NiO)	3−6; 10−20	369; 450; 620	0.814	9.77
Ni/Mg−SBA[23]	27.5	1.64	0.010	14.5 (NiO)	2−4; 20	270; 360; 440; 586	0.874	61.52

[a]BET surface (S_{BET}), average pore diameter (d_{por}), and total pore volume (V_{por}) were obtained from N_2 adsorption isotherm analysis. [b]Average crystalline size (d_{cry}) was estimated by the Scherrer equation from the XRD patterns. [c]The NiO particle size (d_{NiO}) was obtained from TEM images. [d]The maximal reduction temperature (T_{max}) and number of reduced Ni^0 (m_{Ni^0}) were obtained from H_2-TPR results based on H_2 consumption. [e]The desorbed CO_2 amount (m_{Co_2}) was obtained from the CO_2-TPD results.

formed for 100 h TOS was determined by the temperature-programmed oxidation (TPO) in air flow (3 L/h) in velocity. In this process, the temperature was raised from room temperature to 600 °C with a heating rate of 10 °C/min. After that, the temperature was kept at 600 °C for 120 min to ensure complete burning of coke. The coke burning temperature did not exceed 600 °C to avoid damage to the catalyst structure and a change in the physicochemical properties at a high temperature in air.

3. RESULTS AND DISCUSSION

3.1. Properties of Studied Catalysts. The physicochemical properties of the Ni/Mg−Al, Ni/CeO_2, Ni/SBA, and Ni/Mg−SBA catalysts have been already reported in our previous publications[20−22] and are summarized in Table 1 and Figure S1. Briefly, in the NiO catalysts supported on α-Al_2O_3 and CeO_2, nickel oxide exists in an amorphous phase or as highly dispersed crystals.[20,24] Meanwhile, on SBA-15-supported catalysts, NiO exists in the crystalline phase,[23] which was characterized by diffraction peaks at 2θ = 37.3°, 43.3°, and 62.9° corresponding to the (111), (200), and (220) planes of cubic NiO (JCPDS 78-0643), respectively (Figure S1a). The average crystallite sizes of NiO determined from the XRD patterns using Scherrer's equation at 2θ = 43.3° are 18.4 nm in Ni/SBA and 14.5 nm in Ni/Mg−SBA catalysts. The α-Al_2O_3 and CeO_2 supports are in the crystalline phase characterized by diffraction peaks at 2θ = 25.5°, 35.1°, 37.8°, 43.32°, 52.5°, 57.5°, 61.3°, 66.5°, 68.2°, and 76.8° (JCPDS 46-1215) and 2θ = 28.5°, 33.1°,47.5°, 56.4°, 59.1°, 69.4°, 76.7°, and 79.1° (JCPDS 34-0394), respectively. Meanwhile, the silica framework of the SBA-15 support is verified by the broad amorphous silica peak located at 20−30°[25] on the XRD patterns of two SBA-15-supported catalysts.[22,23]

On the Ni/Mg−Al catalyst (Figure S1a), magnesium exists in the form of MgO crystallites at 2θ = 36.9°, 42.9°, 62.3°, 74.7°, and 78.6°) (JCPDS 79-0612 and the mixed metal oxide phase ($Mg_xNi_{1-x}O$) at 2θ = 19.1°, 31.5°, and 65.4°.[26] Furthermore, according to the intensity of the reduction peak on the H_2-TPR profiles (Figure S1b), nickel exists mainly in the mixed metal oxide phase ($Mg_xNi_{1-x}O$) with a maximum reduction temperature (T_{max}) of 875 °C[27] and in a small amount in the form of NiO with T_{max} = 337 °C.[8] The existence of the $Mg_xNi_{1-x}O$ phase on this catalyst is consistent with the results of XRD analysis and also proved by the appearance of thin films in the TEM image.[20] Meanwhile, in the XRD pattern of NiO/Mg−SBA (Figure S1a), the characteristic peaks for MgO crystals and a solid mixture of NiO−MgO at $2\theta \approx 37°$ and 62.4°[28] are very weak, suggesting a high dispersion of magnesium oxide on the support.

On the Ni/CeO_2 sample, nickel species exist in three forms: small particles in the outer pore surface strongly interacting with CeO_2, small particles in the inner pores, and bulk NiO, which are reduced at maximal temperatures of 330, 352, and 395 °C respectively[21] (Figure S1b). On the basis of the area of the reduction peaks, it was asserted[21] that NiO particles located inside the pores are dominant, resulting in the high sintering resistance of the Ni/CeO_2 catalyst. On this sample ceria occurs as CeO_2 or $NiCeO_2$ spinel, which is reduced at 816 °C. Furthermore, the existence of the cubic fluorite phase of CeO_2 is confirmed by the strong peak located at around 450 cm^{-1}[29] in the Raman spectra of the Ni/CeO_2 sample[21] (Figure S1c). Introduction of Ni ions into the ceria cubic fluorite structure increases the thermal stability of poorly thermostable CeO_2.[30] Besides, the presence of oxygen vacancies on the Ni/CeO_2 catalyst are proved by a broad weak reduction peak at around 250 °C on the H_2-TPR profiles[31] and by the appearance of the bands around 625 cm^{-1}[32] on the Raman spectrum.[21] The existence of oxygen vacancies on the Ni/CeO_2 catalyst can create a unique surface state which enhances the surface Ce atom exposure and improves the stability of the catalyst.[33]

Compared to the nonpromoted Ni/SBA sample, all reduction peaks for Mg-promoted Ni/SBA shift toward lower temperature and the amount of Ni° reduced was higher (Figure S1b). This means that the reducibility of the Ni/SBA catalyst is enhanced by introduction of MgO due to the reduction of the crystalline size and particle size of the Ni/Mg−SBA sample (Table 1). In addition, a small new reduction peak appearing at 270 °C shows the reduction of easily reducible NiO species, which have the weakest interaction with the support.[7] This fact is consistent with the absence of a solid mixture of NiO−MgO phase in the Ni/Mg−SBA catalyst as demonstrated in the XRD analysis. Besides, the distribution of types of NiO species changes drastically when MgO is added in the catalyst. In the nonpromoted Ni/SBA sample, nickel species exist mainly in bulky NiO sitting outside of the SBA-5 channels (the first reduction peak is dominant) (Figure S1b). Meanwhile, on the Ni/Mg−SBA catalyst, three types of NiO species, outer bulk NiO, NiO particles strongly interacting with support, and NiO particles anchored inside the channels of SBA-15, exist approximately in the same amount. At the same time, the average crystal size and particle size of NiO decrease, demonstrating that MgO increases the dispersion of NiO.

The SEM and TEM images (Figure S2) demonstrate that the rod-shaped structure of CeO_2 still exists in the Ni/CeO_2 sample.[24] The preservation of the ordered hexagonal channels of the SBA-15 support after impregnation of nickel and magnesium precursors and high-temperature treatments[22,23] ensures the good stability of the prepared SBA-15 support. However, the shift of the diffraction peak at 2θ = 0.9° to a higher value (2θ = 1.1°) on the narrow-angle XRD pattern of Ni/SBA[22] indicates the grafting of NiO onto SBA-15. Due to

https://doi.org/10.1021/acsomega.2c01931
ACS Omega 2022, 7, 20092−20103

the nanorod structure of CeO_2 and the highly ordered channels of the SBA-15 support there are two types of NiO particles existing on the CeO_2 and SBA-15 supports, namely, NiO particles located inside of the pores with a size of 2−6 nm and outer NiO particles having large and various sizes (10−20 nm). The successful dispersion of the metallic species inside of the ordered pores of the CeO_2 nanorods and SBA-15 restrains their mobility due to the confinement effect that enhances the sintering resistance of the catalysts. Meanwhile, NiO aggregating into a big lump of 20−30 nm on the α-Al_2O_3 support was found.[20]

The average pore diameter of MgO-promoted catalysts is much smaller than that of nonpromoted catalysts, as seen from Table 1. Specifically, compared with the corresponding nonpromoted samples, the d_{por} of the Ni/Mg−Al sample decreases 2 times (from 4.0 to 2.02 nm) and that of Ni/Mg−SBA drops 3.7 times (from 6.08 to 1.62 nm). The cause might be due to the incorporation of a MgO particle onto the pore channels of the support. Of the studied samples, the Ni/SBA catalyst possesses the largest average pore diameter and pore volume, reaching 6 nm and 0.291 cm^3/g, respectively, while the other three catalysts have a d_{por} value of about 2 nm and much smaller V_{por}. Even so, with this pore size, the diffusion of CO_2 and CH_4 into the pores of all samples is favorable since the kinetic diameters of CO_2 and CH_4 are 0.33 and 0.38 nm, respectively.[34]

It can be inferred from the results in Table 1 that there is proportionality between the specific surface area of the carriers and the optimal loading of the active phase. The larger the value of S_{BET} of the support, the higher the optimal loading of Ni and the higher the number of reduced Ni° ($m_{Ni°}$) obtained. The BET surface area of the SBA-15 support (639.1 m^2/g[35]) is much larger than those of CeO_2 (71.8 m^2/g)[24] and α-Al_2O_3 (13.4 m^2/g).[20] Therefore, the optimal Ni loading on SBA-15 is the highest, and the number of reduced Ni° ($m_{Ni°}$) of this sample is several times higher than catalysts supported on CeO_2 and α-Al_2O_3 (0.814 vs 0.266 and 0.124 mmol/g). Although adding MgO additive results in a decrease of the specific surface area of the Ni/Mg−SBA catalyst (from 232.6 to 27.5 m^2/g), the amount of reduced Ni increases slightly (about 7%). This is explained by the fact that the Mg promoter increases the dispersion of NiO by reducing the crystal size and particle size of NiO. This results in an improved reducibility of the catalyst (as lower reduction temperatures are required and higher amounts of reduced Ni are obtained).

On all catalysts weak, moderate, and strong basic sites exist, of which the weak basic sites predominate.[20−23] Thus, from the obtained results in Table 1, the decreasing order of the basicity of the catalysts is as follows: Ni/Mg−SBA ≫ Ni/CeO_2 > Ni/SBA > Ni/Mg−Al. The outstanding high basicity of the Ni/Mg−SBA sample can be attributed to the contribution of the alkaline additive MgO and the small particle size caused by the superior specific surface area of the support and the highly ordered channel structure of SBA-15. The relatively high basicity of the Ni/CeO_2 catalyst can be explained by the adsorption of CO_2 on surface Ce^{4+} and Ce^{3+} ions to form carbonate species (CO_3^{2-}).[36] In addition, the oxygen vacancies of CeO_2 stimulate the migration of oxygen in the crystal and increase the electron density in the nano-CeO_2 structure[37] that raises the amount of basic sites.[38] Besides, the good dispersion of NiO particles in the Ni/CeO_2 sample caused by the interaction of Ni^{2+} with the CeO_2 carrier forming Ce^{3+} ions and oxygen vacancies[39] has a significant effect on the surface basicity.[40] As seen from Table 1, modifying the Ni/SBA catalysts with MgO successfully generated numerous basic sites and greatly improved the Ni dispersion (d_{par} and d_{cry} were reduced). The high basicity of the Ni/Mg−SBA, Ni/SBA, and Ni/CeO_2 samples would cause them to have superior coke resistance.

3.2. Catalytic Activity of Studied Catalysts. Figure 1 shows that the activity of the fresh catalysts, evaluated by CH_4 and CO_2 conversions, is high in the BRM reaction. However, CH_4 conversion is always slightly higher than that of CO_2 over the reaction temperature range, suggesting that decomposition of methane into hydrogen and carbon (eq 4),[12] water−gas shift (WGS) (eq 5),[12] and CO disproportionation (eq 6)[41] take place as side reactions.

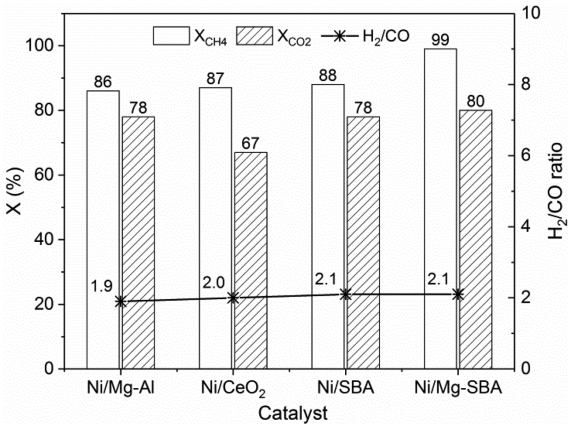

Figure 1. Conversion of CH_4 (X_{CH4}) and CO_2 (X_{CO2}) of fresh catalysts in the BRM reaction at 700 °C.

$$CH_4 \rightarrow 2H_2 + C \quad \Delta H_{298} = 74.87\ kJ/mol \tag{4}$$

$$CO + H_2O \rightleftharpoons H_2 + CO_2 \quad \Delta H_{298} = -41.2\ kJ/mol \tag{5}$$

$$2CO \rightleftharpoons CO_2 + C \quad \Delta H_{298} = -172.44\ kJ/mol \tag{6}$$

In addition, the reaction heat of steam methane reforming (eq 1) is smaller than that of dry methane reforming (eq 2) (+206.3 vs +247.3 kJ/mol), so CH_4 being converted in reaction 1 is more favorable, and as a result, the conversion of CH_4 is higher than that of CO_2.

At 700 °C, CH_4 conversion is 86−99% while that of CO_2 is 67−80%, in which the Ni/Mg−SBA catalyst has the best activity with conversion of CH_4 and CO_2 reaching 99% and 80%, respectively. The catalyst activity has a good relation with the Ni dispersion.[42] Thus, the high dispersion of the nickel species and more reducible NiO nanoparticles present in the Ni/Mg−SBA catalyst, in line with the highest porosity and basicity (Table 1), contribute to the highest performance of this catalyst compared to the other samples. Furthermore, much more basic sites on the Ni/Mg−SBA catalyst's surface contributes to better adsorption of CO_2, implicating better conversion of CO_2.[43] However, CO_2 conversion on the Ni/Mg−SBA catalyst is almost no different from that on the Ni/SBA sample, as shown in Figure 1. This might be related to the high ability of CO oxidation to CO_2 by alkaline earth metal Mg[44] and CO disproportionation (eq 6) on MgO,[45] resulting in a reduction of CO_2 conversion.

The smallest CO_2 conversion being obtained on the Ni/CeO_2 catalyst is explained by the fact that the interaction

https://doi.org/10.1021/acsomega.2c01931
ACS Omega 2022, 7, 20092−20103

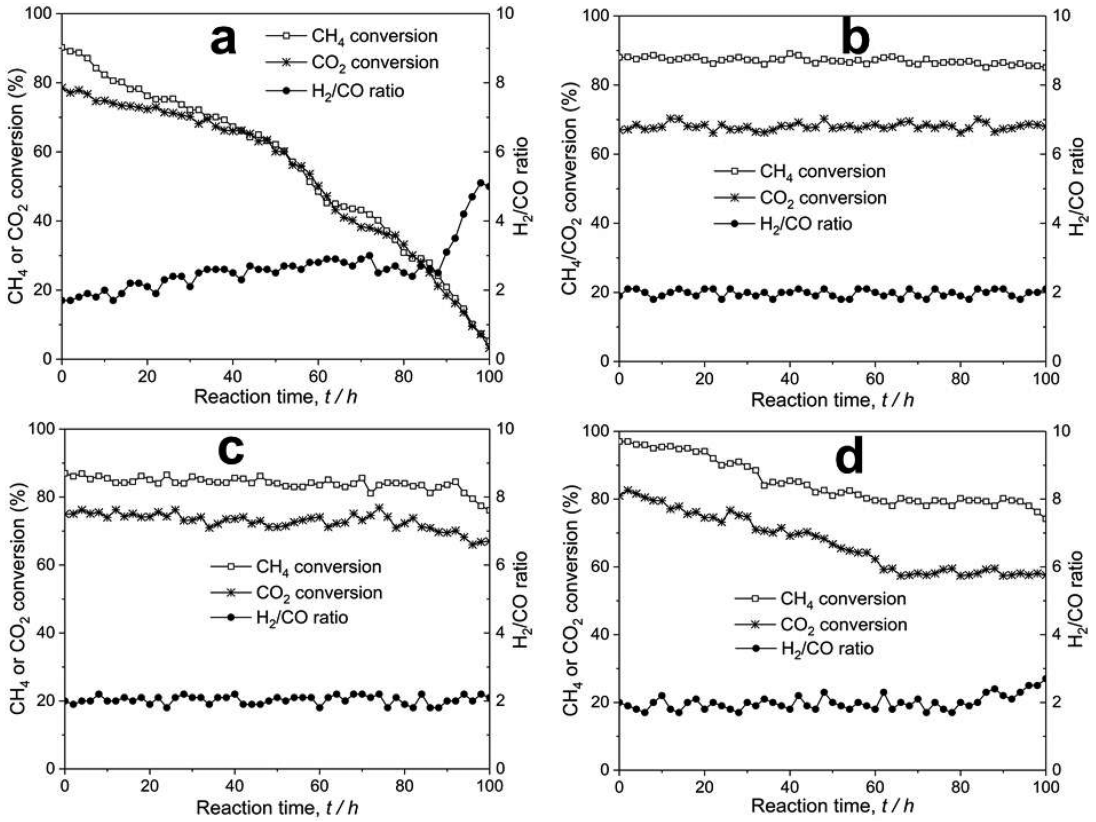

Figure 2. Activity of samples: (a) Ni/Mg−Al, (b) Ni/CeO_2, (c) Ni/SBA, and (d) Ni/Mg−SBA at 700 °C for 100 h TOS.

between the deposited carbon and the lattice oxygen of CeO_2 on this sample would lead to the formation of C, O[46] which then reacts with steam to produce H_2 and CO_2. After that H_2 and CO_2 are involved in the WGS reaction (eq 5) because the reducible oxides such as CeO_2, doped-CeO_2, and ZrO_2 show high activity in the WGS reaction.[47] Hua Zang et al.[48] also found that Fe−Ce−Ni-based oxygen carriers have a remarkable redox behavior and exerted high activity and stability for coproduction of hydrogen and syngas from chemical looping water splitting (CLWS) coupled with glycerol decomposition.

Regarding the H_2:CO molar ratio, it was 1.9 on Ni/Mg−Al, around 2.0 on Ni/CeO_2, and 2.1 on two SBA-15-supported catalysts. The low H_2:CO molar ratio in the BRM reaction on Ni/Mg−Al is attributed to the reverse water−gas shift (RWGS) reaction[41] since nonreducible oxides (Al_2O_3 or MgO) are active promoters for RWGS reaction.[47] Specifically, alkali metals intensify the electrostatic interactions by promoting electron transfer with reacting molecules that enhance the CO_2 adsorption capacity.[49] An approximate value of 2 on the Ni/CeO_2 catalyst indicates that on this catalyst the side reaction is negligible. Recently, the development of a bimetallic catalyst system based on Ni/CeO_2 for H_2 production has been proposed. It was found that the Cu element in the Ni−Cu bimetallic supported on mesoporous CeO_2 catalysts can effectively improve the water−gas shift reaction and inhibit the formation of methane in aqueous phase reforming (APR), which increases the H_2 production rate.[50]

The higher molar ratio of H_2:CO (2.0) on the Ni/SBA sample can be attributed to the WGS reaction, while the decomposition of methane (eq 4) and/or Boudouard reaction (eq 6) on Ni/Mg−SBA are responsible for this high value. As reported, Mg is an active promoter for CO disproportionation.[45] It was reported that NiO and CeO_2 in mesoporous oxygen carriers (OCs) such as SBA-15 and MCM-41 were first reduced by fuels and that the reduced OCs was responsible for steam reforming and water−gas shift reaction (eq 5) to hydrogen production, and hydrogen selectivity was up to 90% using CeNiO/SBA-15.[51]

3.3. Catalytic Stability with Time on Stream. The long-term stability test in the BRM reaction was conducted on the catalysts for continuous reactor operation at 700 °C for 100 h, while conversion was monitored continuously. The reaction results for CH_4 and CO_2 conversion with time on stream are presented in Figure 2.

It can be seen in Figure 2 that both Mg-containing samples are not stable with the reaction time in the BRM reaction. The activity of the Ni/Mg−Al catalyst (Figure 2a) decreases rapidly for 100 h TOS in the BRM reaction. The conversion of both CH_4 and CO_2 drops sharply from 86% and 78%, respectively, to approximately 2% after 100 h TOS. Meanwhile, it was reported by Roh et al. that the higher activity and stability of Ni/MgO−Al_2O_3 compared to nonpromoted catalyst Ni/Al_2O_3 is due to the beneficial effects of MgO such as enhanced steam adsorption, basic properties, nanosized NiO crystallite, and strong interaction between Ni and the support.[19] Simultaneously, the activity of the modified catalyst Ni/MgO−Al_2O_3 was stable for 20 h of testing, while the activity of the Ni/Al_2O_3 sample decreased by 60% in the first 5 h of the reaction.

On the Ni/Mg−SBA catalyst, as observed in Figure 2d, CO_2 conversion gradually decreases from 80% to 60% while CH_4 conversion decreases slowly from 97% to around 80% in 100 h TOS. Besides, the H_2/CO molar ratio increases rapidly from 1.9 to 5.0 on the first catalyst and from 2.1 to 2.2 on the

https://doi.org/10.1021/acsomega.2c01931
ACS Omega 2022, 7, 20092−20103

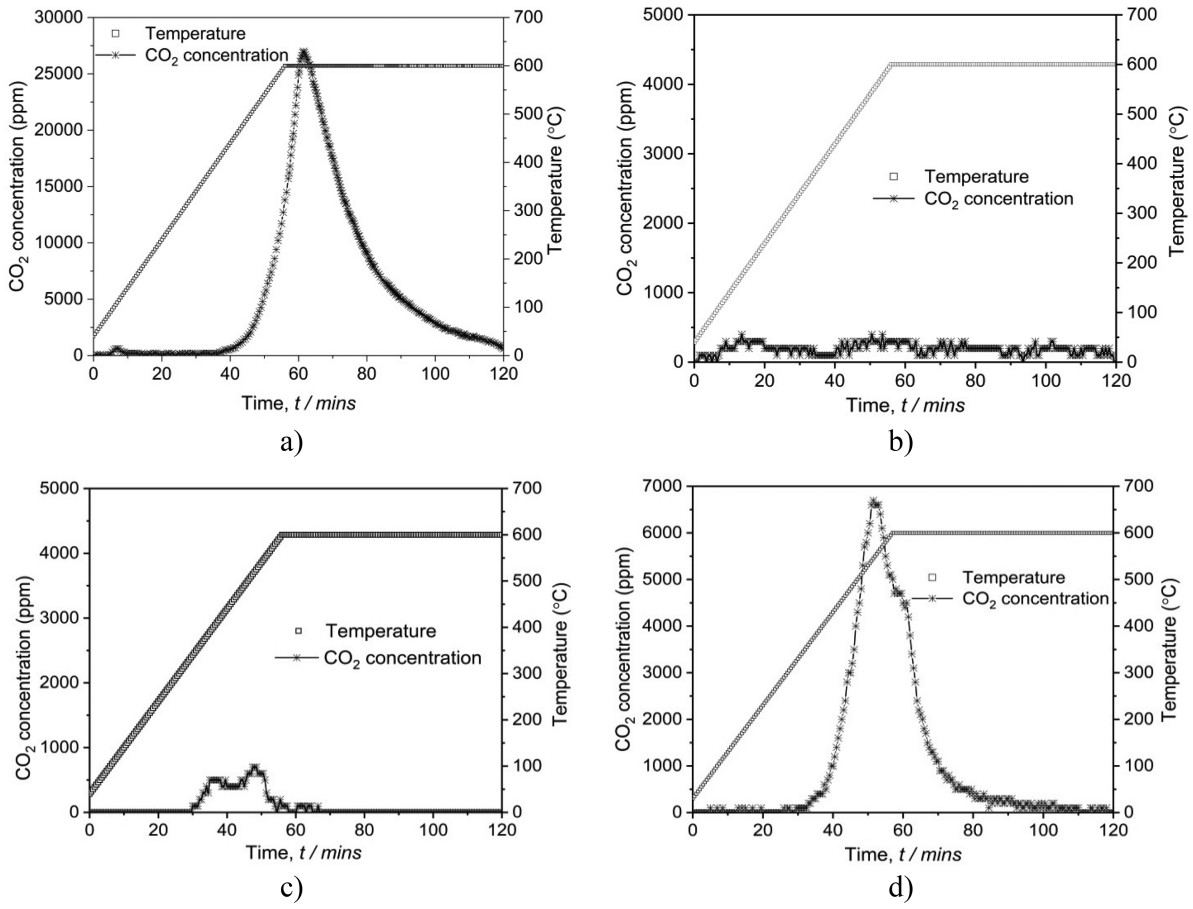

Figure 3. Temperature-programmed oxidation patterns of spent catalysts: (a) Ni/Mg−Al, (b) Ni/CeO_2, (c) Ni/SBA, and (d) Ni/Mg−SBA catalysts after 100 h TOS at 700 °C.

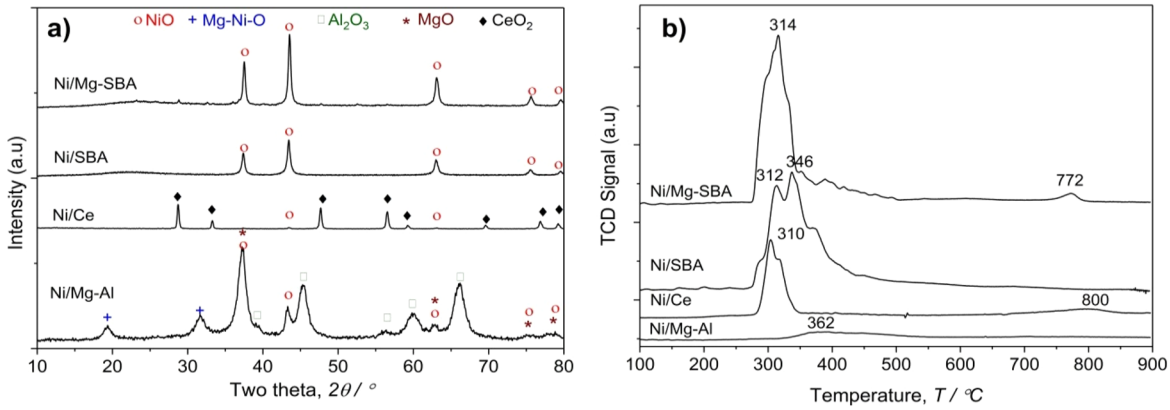

Figure 4. XRD patterns (a) and H_2-TPR patterns (b) of the spent catalysts.

second one. The remarkable increase in the H_2:CO ratio shown on the Ni/Mg−Al catalyst with the reaction time could be explained by the acceleration of methane decomposition to produce hydrogen (eq 4), Boudouard reaction (eq 6), and the limitation of the RWGS reaction, which leads to CO_2 production and carbon accumulation. The enhancement of the Boudouard reaction and the decline of the RWGS reaction may be due to the promoting role of MgO in CO_2 adsorption during the reaction since both of them are facile on MgO.[49] Regarding methane decomposition, it can occur at temperatures as low as 500−750 °C in the presence of catalysts.[52] A decrease in activity with reaction time was also observed on the Co-modified Ni/Mg−SBA-15 catalyst in the DRM reaction. In methane CO_2 reforming, CH_4 conversion on the Co−Ni/Mg−SBA-15 catalyst decreased slowly in the first 20 h and then decreased sharply; after 51 h of reaction, CH_4 conversion decreased from 84% to 50%.[7]

Meanwhile, the Ni/CeO_2 (Figure 2b) and Ni/SBA (Figure 2c) catalysts demonstrate stable conversion of CH_4 (roughly 87% and 88%) and CO_2 (almost 67% and 78%) for 100 h TOS, and the ratio of H_2/CO is kept approximately at the theoretical value of 2.0 for the Ni/CeO_2 catalyst and 2.1 for the Ni/SBA catalyst. The increasing rate of the H_2:CO ratio on these two catalysts with reaction time is insignificant, indicating

https://doi.org/10.1021/acsomega.2c01931
ACS Omega 2022, 7, 20092−20103

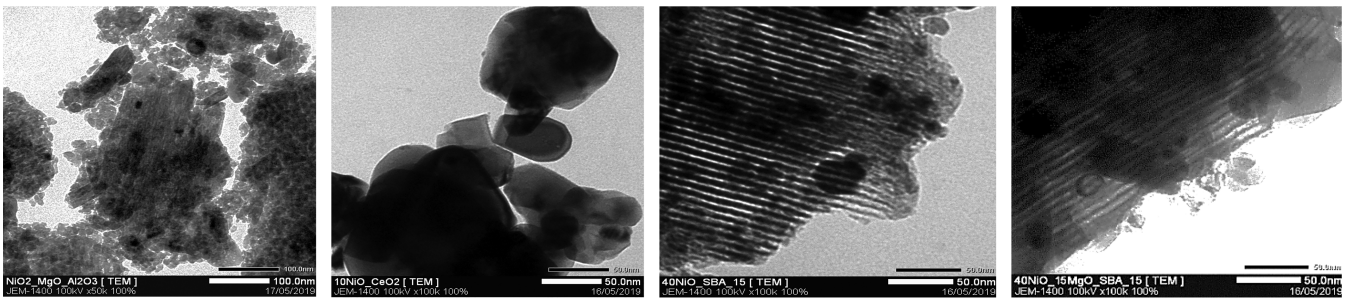

a) b) c) d)

Figure 5. TEM images of the spent catalysts: (a) NiMg/Al, (b) Ni/CeO_2, (c) Ni/SBA, and (d) NiMg/SBA.

that the side reactions (eqs 4−6) take place with a lower rate, probably leading to low coke accumulation and stable activity. These facts prove that the Ni/CeO_2 and Ni/SBA catalysts have good stability in the BRM reaction.

The deactivation of the catalysts could be well understood in conjunction with the results of the carbon deposits (Figure 3) and the characteristics of the spent catalysts (Figures 4 and 5).

3.4. Coke Formation on the Catalysts after 100 h TOS. On the basis of the TPO patterns of the spent catalysts after 100 h TOS at 700 °C (Figure 3), the amount of CO_2, corresponding to the amount of coke formed, could be determined. The Ni/CeO_2 and Ni/SBA catalysts had a very low coke amount formed after 100 h TOS, being nearly ∼0.30 and 0.43 $mgC \cdot g_{cat}^{-1}$, respectively (Figure 3b and 3c). Meanwhile, on two samples containing MgO (Ni/Mg−Al and Ni/Mg−SBA) (Figure 3a and 3d), the amount of coke formed after 100 h TOS is much bigger, 7.70 and 1.73 $mg_C \cdot g_{cat}^{-1}$ respectively.

There are three forms of carbon deposited during methane reforming, amorphous and highly reactive mono carbon (denoted as C_α), unstable β-carbon species (C_β), and graphitic/inert carbon (C_γ), correlating with the hydrogenation peaks at around 178, 485, and 655 °C, respectively.[25] C_α is considered to be an active species, which easily reacts with CO_2 to produce CO during the carbon dioxide reforming of methane.[53] In the TPO pattern of spent Ni/Mg−Al catalyst (Figure 3a), one strong peak appearing at 600 °C attributed to graphitic/inert carbon (C_γ) was seen. Meanwhile, on the Ni/Mg−SBA catalyst, there is a main peak with a maximum at 550 °C and a shoulder at 600 °C, representing the unstable β-carbon species (C_β) and graphitic/inert carbon (C_γ), respectively, in which C_β predominates as seen from Figure 3d. On the Ni/SBA catalyst, two peaks appeared in the low-temperature region, around 80 and 100 °C, belonging to the highly reactive mono carbon (C_α) category (Figure 3c), while the TPO pattern of the ceria-supported catalyst (Ni/CeO_2) shows almost no peak (Figure 3b).

The results of Figures 2 and 3 show that there is a corresponding relationship between the growth rate of the H_2:CO molar ratio with the reaction time, coke deposition, and catalyst stability. The order of catalysts based on the amount of coke accumulated after 100 h of TOS and the growth rate of the H_2:CO molar ratio with reaction time is as follows Ni/Mg−Al ≫ Ni/Mg−SBA > Ni/SBA ≈ Ni/CeO_2, while the catalysts' stability is in the reverse order. The sharp rise of the ratio of H_2:CO with TOS indicates that the side reactions increase significantly during the process due to the change in the physicochemical properties of the Ni/Mg−Al catalyst. Furthermore, among the side reactions, the methane decomposition (eq 4) and Boudouard (eq 6) reactions generate significant amounts of coke.

In the methane reforming reaction, deposited carbon originates from CH_4 decomposition (eq 4) and CO disproportionation (eq 6).[54] Normally, at reaction temperatures above 800 °C, the highly active coke originating from the decomposition of CH_4 is easily oxidized by CO_2.[55] However, at 700 °C, the CH_4 decomposition rate is higher than the oxidation rate of coke with CO_2. Thus, coke accumulation increases.[56] In this study, on the Ni/CeO_2 catalyst almost no coke is formed after 100 h of the BRM reaction even at 700 °C. The reason is that possible coking in the Ni/CeO_2 catalyst is lessened due to the reaction of surface carbon species with the lattice oxygen or the surface O species (O*) as produced from CO_2 or H_2O in the reaction with oxygen vacancies (*).[57] The oxygen vacancies increase not only the CO_2 dissociation activity but also the conversion of the adsorbed carbon species, i.e., CH_x, via the oxygen-transport reaction. This greatly increases the CH_4 conversion, which produces hydrogen, and also lessens the carbon deposition. At the same time, the CO_2 conversion rate is further enhanced due to consumption of the produced oxygen species. As a result, the H_2:CO ratio remains constant at around 2, as indicated in Figure 2b.

The high dispersion of Ni (small d_{NiO}) and high number of reduced Ni° ($m_{Ni°}$) (Table 1) cause the methane decomposition to take place,[58] generating unstable α-carbon species on the used Ni/SBA sample, which easily reacted with CO_2 to produce CO in a reverse Boudouard reaction during the BRM reaction at 700 °C.[53] Furthermore, the improvement of the oxygen storage capacity/mobility on well-ordered structure SBA-15 resulted in its high catalytic activity and resistance to coke formation.[7]

The TPO results indicate that the presence of γ-carbon was associated with the deactivation of Ni/Mg−Al and Ni/Mg−SBA-15. The formation of γ-carbon on the Ni/Mg−Al catalyst indicated that on this catalyst coke is formed mainly in the Boudouard reaction (eq 6), producing inactive carbon. This is completely consistent with the fact that Ni/Mg−Al is the catalyst with the least basic sites density among the studied catalysts (Table 1), leading to low CO_2 adsorption. The presence of γ-carbon associated with deactivation of the Ni/SBA-15 and Ni/Mg−SBA-15 catalysts was found in a prior investigation.[25] Besides, formation of large Ni particles (Table 1) also resulted in heavy coke deposition[10] on the Ni/Mg−Al catalyst.

The lower occupancy of active sites by γ-carbon over Ni/Mg−SBA compared to Ni/Mg−Al led to better catalytic stability as seen in Figures 2 and 3. Thanks to the highest

https://doi.org/10.1021/acsomega.2c01931
ACS Omega 2022, 7, 20092−20103

amount of reduced Ni°, on the Ni/Mg−SBA catalyst the methane decomposition reaction (eq 4) takes place strongly, producing carbon C_β, which is rapidly gasified in the reverse Boudouard reaction (eq 6). Since much less γ-carbon is deposited, the coke accumulation rate is lower on the spent Ni/Mg−SBA sample, being 1.72 mg_C/g, 3.5-fold lower than that of the Ni/Mg−Al catalyst. Therefore, the total reduction of the conversion of both CH_4 and CO_2 after 100 h with the Ni/Mg−SBA catalyst was not more than 15−20% and remained at high values of 80% and 60%, respectively. The much higher specific area (almost 3.9-fold), reducibility (7-fold), and basicity of the Ni/Mg−SBA catalyst relative to the Ni/Mg−Al catalyst might be responsible for its higher stability. Moreover, the larger dispersed Ni particle size on the Ni/Mg−SBA sample (d_{NiO} of 2−4 vs 20−30 nm for Ni/Mg−Al, as seen in Table 1) increased the adsorption of CO_2, exhibiting a higher reforming activity, lower coke formation, and higher catalytic stability.[59]

Compared with the Ni/SBA catalyst, the Ni/Mg−SBA-promoted catalyst had lower stability and coke resistance. This is explained as follows. The enhanced basicity by the incorporation of a Mg promoter, as shown in Table 1, is advantageous as the CO_2 adsorption affinity can be ameliorated, which in turn affects the CO_2 conversion and subsequently suppresses the coke accumulation at the catalyst surface that enhanced the activity stability.[2,28] However, it was indicated that the excessive basicity of the catalyst itself is detrimental to the catalytic activity as it will stimulate a higher extent of the CO_2 dissociation into C and O_2 and therefore deactivate the catalyst.[60] The influence of this reaction further worsens the stability and coke resistance of the catalyst when the Boudouard reaction occurs simultaneously. Thus, it was deduced that compared to the Ni/SBA catalyst, Ni/Mg−Al and Ni/Mg−SBA were less favorable for the BRM reaction due to their insufficient and excessive basicity. The investigation results of Al-Fatesh et al. also confirmed that the Mg and Sc additives increased the coke accumulation of the Co−Ni/SBA-15 catalysts in the DRM reaction.[7] The amount of coke formed after 51 h TOS of the DRM reaction decreases in the order Co−Ni/Mg−SBA−15 > Co−Ni/Sc-SBA-15 > Co−Ni/SBA-15 > Co−Ni/La-SBA-15.

In fact, the coke formation rate and the type of carbon deposits are the reasons for the catalyst deactivation. The higher basicity and smaller NiO particle size of three catalysts, Ni/CeO_2, Ni/SBA, and Ni/Mg−SBA, can inhibit the nucleation and growth of inert carbon (C_γ),[61] which bestowed their superior coke resistance over the Ni/Mg−Al sample.

3.5. Physicochemical Properties of Spent Catalysts after 100 h TOS. The XRD pattern of the spent Ni/Mg−Al catalyst after 100 h of reaction (Figure 4a) no longer has all of the characteristic diffraction peaks of the crystallite phases. Specifically, the diffraction peaks of α-Al_2O_3 only appear at 2θ = 43.3° and 66.5°, and its crystallite size significantly drops from 25.6 nm in the fresh sample[20] to ∼7 nm, showing that the crystalline structure of α-Al_2O_3 has been destroyed and/or transformed into the amorphous phase. This is consistent with the TEM image (Figure 5a), showing that the used catalyst is broken into small particles, a few nanometers in size. The XRD diffraction peaks of NiO remain stable in comparison with the fresh sample.[20] Furthermore, in the XRD plot, the peaks for MgO and the mixed metal oxide phase ($Mg_xNi_{1-x}O$) almost disappeared. This may be due to the formation of magnesium carbonates from the MgO−CO_2−H_2O system.[62] This is entirely consistent with the observations from the TEM image of the spent Ni/Mg−Al sample (Figure 5a), where the NiO−MgO solid thin film which exists on the fresh Ni/Mg−Al sample (Figure S2a′) is no longer observed.[20] Instead, the spent catalyst exists in the form of discrete, nonporous particles, and the NiO active phase appears mainly on the surface in aggregate form because of sintering (Figure 5a). Simultaneously, in the H_2-TPR pattern of the spent Ni/Mg−Al sample (Figure 4b), the reduction peak of the mixed metal oxide phase ($Mg_xNi_{1-x}O$) is no longer observed at T_{max} = 850 °C.[20] These facts show that the crystalline structure of α-Al_2O_3 in the Ni/Mg−Al catalyst has changed after 100 h TOS of the BRM reaction. Moreover, the H_2-TPR pattern of the spent Ni/Mg−Al catalyst markedly changes compared to the as-prepared sample.[20] More specifically, a large reduction peak appears in the temperature range of 325−525 °C, which is typical for the reduction of free bulk NiO instead of the reduction peak of small particles NiO, which appeared at 337 °C on the fresh sample (Figure S1b). In addition, the amount of reduced Ni° calculated from the H_2-TPR pattern decreases 2-fold from 0.112 to 0.064 $mmol{\cdot}g_{cat}^{-1}$ after 100 h TOS. The weakening of the strong Ni−support interaction worsens the dispersion of NiO, resulting in a sharp decrease in the catalytic activity. Moreover, the free NiO species, which has no interaction with the support, is responsible for coke formation in methane reforming,[63] resulting in catalyst deactivation.[16]

In contrast, after 100 h TOS, the XRD pattern of the Ni/CeO_2 sample (Figure 4a) is unchanged; all of the peaks characteristic of CeO_2 crystals still appear, although their intensities are weakened, and the CeO_2 crystal size is increased slightly from 23.7 to 26.5 nm. In addition, the XRD spectrum of the used Ni/CeO_2 catalyst (Figure 4a) does not show any new diffraction peaks relative to the fresh one, indicating that no new phase is generated in the sample. After 100 h of reaction, the H_2-TPR pattern of the Ni/CeO_2 spent catalyst (Figure 4b) shows a sharp reduction peak at ∼310 °C and a shoulder at 350 °C, which are attributed to the reduction of small-sized NiO particles outside and inside of the pores that strongly interact with CeO_2, respectively.[64] Thus, diffusion of the NiO particles from inside the pore to the outer surface takes place during the reaction. Therefore, the NiO species exist mainly in the form of external small-sized particles strongly interacting with the support. The high-temperature reduction peak (T_{max} = 800 °C), which is typical for the reduction of oxygen in the lattice CeO_2 support or $NiCeO_2$ spinel,[65] appears in both the fresh and the used Ni/CeO_2 samples, demonstrating the thermal stability of CeO_2 in the Ni/CeO_2 catalysts for 100 h TOS despite the poorly thermal stability of CeO_2[66] thanks to the introduction of Ni^{2+} ions into the ceria cubic fluorite structure.[30] Although the CeO_2 particles are still discretely dispersed, binding of some CeO_2 rods into larger lumps after 100 h TOS has taken place, as shown in the TEM image (Figure 5b), resulting in the weakness of the NiO−CeO_2 interaction. As a result, the maximum reduction temperature of the three main reduction peaks is shifted to a lower temperature region relative to the fresh Ni/CeO_2 catalyst. However, the disappearance of the reduction peak of massive NiO (T_{max} = 390 °C) shows that despite the weakening the NiO−support bond, the NiO particles are still highly dispersed. As a result, on this catalyst, the amount of Ni° formed in the reduction process decreases at a low rate, less than 18%, from 0.266 $mmol{\cdot}g^{-1}$ in the fresh catalyst to 0.216 $mmol{\cdot}g^{-1}$ in the used sample. Thus, the

https://doi.org/10.1021/acsomega.2c01931
ACS Omega 2022, 7, 20092−20103

results of XRD, H_2-TPR analysis, and TEM prove that the structure of CeO_2 is preserved after the reaction at high temperature. The existence of oxygen vacancies and the redox property of the lattice CeO_2 (expressed in T_{max} = 800 °C) maintain the continuous combustion of carbon deposited on the catalyst's surface. Moreover, the reduction degree of Ni^{2+} ions is still high, contributing to the maintenance of the catalyst activity at a high and stable value.

The XRD pattern (Figure 4a) of the spent Ni/SBA sample is quite similar to that of the fresh one,[22] having characteristic peaks for the NiO crystal at 2θ = 37.3°, 43.3°, and 62.9°. The broad amorphous silica peak located at 20−30° still appears in the XRD pattern of the spent Ni/SBA catalyst, proving the existence of the frame SBA-15 support.[25] Furthermore, the highly order channel structure of SBA-15 is observed in the TEM image of the spent Ni/SBA catalyst (Figure 5c). These are evidence of the structural stability of the Ni/SBA catalyst after undergoing a high-temperature reaction for 100 h thanks to the high thermal stability of SBA-15.[19] In the TEM image of the spent Ni/SBA sample (Figure 5c) it is observed that there are NiO particles located inside and outside of the channels of SBA-15 with sizes of about 6 and 15−25 nm, respectively. The size of the two types of NiO particles increases insignificantly thanks to the distinct properties (high specific surface area, uniform narrow pore size distribution, confinement effect, ...) of SBA-15 favoring metal dispersion and limiting particle sintering.[10,12] This change in the distribution of the NiO particles is clearly reflected in the reduction characteristics of the spent Ni/SBA catalyst. Indeed, the H_2-TPR pattern of the spent Ni/SBA catalyst (Figure 4b) shows the appearance of two reduction peaks at $T_{max,1}$ = 312 °C and $T_{max,2}$ = 346° and a shoulder at 369 °C. Two first main reduction peaks are assigned to the reduction of external NiO species of small and large size that weakly interact with the support, respectively. The shoulder at 369 °C is attributed to the reduction of internal NiO species that moderately interact with the support.[67] In addition, a broad reduction peak appears at $T_{max,3} \approx$ 620 °C in the fresh Ni/SBA catalyst (Figure S1b), which is characteristic of the reduction of a large particle of NiO strongly interacting with the support[25] and/or NiO strongly interacting with the support deep in the pores[68] which are no longer observed on the spent catalyst after 100 h TOS. Generally, on the spent Ni/SBA sample, the maximum reduction temperature of NiO is lower than that in the fresh one. This fact shows that after 100 h of reaction, the interaction between NiO and SBA-15 is weakened and movement of part of the NiO particles from inside to outside of the pores takes place. Moreover, the amount of reduced Ni° negligibly decreases, about 6%, from 0.814 mmol·g^{-1} in the fresh Ni/SBA sample to 0.766 mmol·g^{-1} after 100 h TOS. Thus, the physicochemical properties of the Ni/SBA catalyst still remain after 100 h of reaction at high temperature. Therefore, the catalyst activity is maintained relatively stable during the 100 h TOS.

Regarding the Ni/Mg−SBA catalyst, after 100 h of reaction, the highly ordered channel structure of SBA-15 was also observed in the TEM image (Figure 5d) and the XRD pattern (Figure 4a) does not change; diffraction peaks at 2θ = 37.3°, 43.3°, and 62.9° corresponding to the (111), (200), and (220) planes of cubic NiO (JCPDS 78-0643), respectively, were also observed. This is evidence for the structural stability of the NiO crystals in the Ni/Mg−SBA sample after a long reaction time; however, significant growth of the NiO crystallite size was observed, from 14.5 to 22.6 nm, an increment of ∼8 nm, a bigger change than that on the nonpromoted Ni/SBA sample. This can be directly related to a higher rate weakening the metal−support interaction during the reaction in Ni/Mg−SBA. Further, the H_2-TPR pattern (Figure 4b) of the spent Ni/Mg−SBA catalyst has changed remarkably compared to that of the fresh sample.[23] As seen in Figure 4b, for the spent Ni/Mg−SBA catalyst, two reduction peaks were detected at 314 and 772 °C. The first reduction peak, assigned to reduction of a massive weakly interacting NiO species, shifts toward a lower temperature region compared to that of the fresh sample. This proves that, similar to the three other catalysts, in the Ni/Mg−SBA catalyst the interaction between NiO with the support and MgO weakens during the 100 h tested. The second peak at 772 °C corresponds to the reduction of Ni^{2+} ions with square-pyramidal coordination in the outer layer of the MgO structure or deeply located in the MgO lattice in the spent sample,[25] which newly appears relative to the fresh sample. In addition, as can be seen in the TEM image of the spent Ni/Mg−SBA (Figure 5d), the outer particles have different brightness. It can be assumed that the black spots belong to the NiO particles, while the light-colored ones are assigned to the NiO−MgO mixture, produced from diffusion of nickel into the magnesia lattice[69] due to their very close ionic radius (about a 0.02 Å difference),[70] which was reduced at a high temperature of 772 °C on the TPR pattern. Formation of a solid solution generates small metal clusters during the reaction that are more resistant to sintering and carbon formation.[71] However, the poor reducibility of the NiO−MgO mixture[72] resulted in a lower reducibility of the catalyst from 0.874 to 0.782 mmol·g^{-1}, as shown in Table 2.

Table 2. Textural Properties of the Spent Catalysts

catalysts	d_{cry} [a] (nm)	d_{NiO} [b] (nm)	T_{max} [c] (°C)	$m_{Ni°}$ [c] (mmol/g)
Ni/Mg−Al	6.95 (Al_2O_3)	10−20	320−550	0.064
Ni/CeO_2	26.52 (CeO_2)	3−5; 20−70	290−350; 800	0.216
Ni/SBA	19.73 (NiO)	3−6; 15−25	312; 346	0.766
Ni/Mg−SBA	22.59 (NiO)	3−5; 10−40	314; 772	0.782

[a]Average crystalline size (d_{cry}) was estimated by the Scherrer equation from the XRD patterns [b]The NiO particle size (d_{NiO}) was obtained from the TEM images. [c]The maximal eduction temperature (T_{max}) and number of reduced Ni° ($m_{Ni°}$) was obtained from H_2-TPR results based on H_2 consumption.

Thus, adding MgO significantly enhanced the basicity of the Ni/SBA catalyst, as shown in Table 1, leading to increased adsorption and dissociation of CO_2 into CO and O*; the produced oxygen species promotes the autocatalytic H_2O dissociation,[73] i.e.

$$H_2O + {}^{*} + O^{*} \rightarrow H_2 + 2O^{*} \quad (7)$$

Thus, under the BRM reaction at 700 °C compared with the Ni/SBA catalyst, the Ni/Mg−SBA-promoted catalyst has superior initial activity thanks to the increase in basicity and Ni dispersion but its long-term stability is worse. For a long time operating at high temperature (700 °C) as the concentration of O* increases to some extent, Ni sites become occupied by the O* species; consequently, the reaction slows down.[73] Further, Mg, an alkaline earth metal, may even

https://doi.org/10.1021/acsomega.2c01931
ACS Omega 2022, 7, 20092−20103

disintegrate into the base formation and cover the active site surface from the catalyst structure at high temperature, which resulted in catalyst deactivation.[28] This will get worse when there is diffusion of Ni into the MgO lattice. Thus, for the BRM reaction, an excessive increase in the basicity of MgO can lead to a decrease in catalyst stability.

In summary, the XRD diagram and TEM image confirm that after 100 h of reaction the structure of Ni/Mg−Al changes completely while those of the other three samples, Ni/CeO_2, Ni/SBA, and Ni/Mg−SBA, change slightly. The phase composition of the active component of the MgO-containing catalysts has changed remarkably, while that did not happen in the other two catalysts (Ni/CeO_2, Ni/SBA). However, the reduction in the amount of Ni° reduced of spent sample in comparison with the fresh one is smallest on the SBA-15-supported catalysts, namely, 6% for the Ni/SBA and 10% for the Ni/Mg−SBA samples, moderate on Ni/CeO_2 catalysts (18%), and largest on Al_2O_3-supported catalyst Ni/Mg−Al (∼50%). This result shows that the ability to resist sintering of NiO particles in the catalysts during the reaction depends strongly on the supports used, and their decreasing order is as follows: SBA-15 > CeO_2 > α-Al_2O_3.

The presence of MgO somehow stimulates the formation of inert carbon C_γ, leading to an increase in coke accumulation, reducing the stability of the nickel catalyst in the BRM reaction. Of the catalysts studied, the Ni/Mg−Al sample was shown to be the worst, with the highest coke deposited and the worst stability. Ni/Mg−SBA has the highest activity but lower stability than nonpromoted Ni/SBA and Ni/CeO_2 samples. Comparing the performance of the two SBA-15-supported catalysts, Ni/SBA and Ni/Mg−SBA, in the BRM reaction, it is obvious that adding MgO increases the reducibility, basicity, and dispersion of NiO, leading to an increase in the activity of the catalyst. However, with excess basicity, the MgO-promoted catalyst (Ni/Mg−SBA) has more coke deposited and lower stability in comparison with the nonpromoted one. The high coke resistance and structural and thermal stability of the nickel catalysts supported on CeO_2 and SBA-15 provide these catalysts with excellent stability during 100 h TOS. Thus, it is deduced that Ni/Mg−Al and Ni/Mg−SBA-15 are less favorable for BRM activity due to their insufficient and excessive basicity, respectively.

4. CONCLUSION

The nature and morphology of the supports have a profound influence on the properties of the catalyst, which in turn affect the activity and the rate as well as the type of coke deposited. The highly ordered structure of the CeO_2 nanorod and SBA-15 give catalysts a high NiO dispersion and excellent reducibility and basicity, providing the catalysts with superior activity, stability, and coke resistance due to minimization of the inert carbon C_γ formation. The large surface area, high thermal stability, large pore volume, and uniform mesoporous channels of SBA-15 facilitate high dispersion of the NiO particle, which in turn gives the NiO/SBA-15 catalyst a high resistance to sintering and coke deposition. The highly structural as well as thermal stability of CeO_2 caused by introduction of Ni^{2+} ions into the ceria cubic fluorite structure and the presence of oxygen vacancies in the CeO_2 support result in a high antisintering and superior coke resistance of the Ni/CeO_2 catalyst. Both catalysts have stable activity for 100 h TOS, and there was almost no coke deposited on the catalyst surface after 100 h TOS. MgO additive increases the reducibility, basicity, and dispersion of NiO, resulting in an increase in the activity of the catalyst. At 700 °C, the conversion of CH_4 and CO_2 on the Ni/Mg−SBA catalyst reaches 99% and 80%, respectively. However, addition MgO leads to an acceleration of the inert C_γ carbon deposition and an excessive increase in the basicity that reduces the stability and coke resistance of the Ni/Mg−SBA catalyst in the BRM reaction. The small specific surface area, low basicity, poor reducibility, and low NiO dispersion of the Ni/Mg−Al catalyst result in a low BRM performance and low coke resistance. The catalyst supported on α-Al_2O_3 faces not only a marked change in crystallite structure, morphology, and reducibility but also serious accumulation of inert γ-carbon. These cause the catalytic activity to drop continuously during 100 h of experiment.

ASSOCIATED CONTENT

Supporting Information

The Supporting Information is available free of charge at https://pubs.acs.org/doi/10.1021/acsomega.2c01931.

Crystalline phase patterns (powder X-ray diffraction), reducibility (H_2 temperature-programmed reduction, H_2-TPR, profiles), basicity (temperature-programmed desorption of CO_2, CO_2-TPD, profiles), Raman spectra of the Ni/CeO_2 catalyst, and morphology (scanning electron microscope, SEM, and transmission electron microscopy, TEM) of fresh catalysts (PDF)

AUTHOR INFORMATION

Corresponding Author

Luu Cam Loc − *Faculty of Chemical Engineering, Ho Chi Minh City University of Technology (HCMUT), Ho Chi Minh City 701000, Vietnam; Vietnam National University Ho Chi Minh City, Ho Chi Minh City 701000, Vietnam; Institute of Chemical Technology−Vietnam Academy of Science and Technology, Ho Chi Minh City 701000, Vietnam;* orcid.org/0000-0001-8821-5433; Email: lcloc@ict.vast.vn

Authors

Phan Hong Phuong − *Faculty of Chemical Engineering, Ho Chi Minh City University of Technology (HCMUT), Ho Chi Minh City 701000, Vietnam; Vietnam National University Ho Chi Minh City, Ho Chi Minh City 701000, Vietnam*

Ha Cam Anh − *Faculty of Chemical Engineering, Ho Chi Minh City University of Technology (HCMUT), Ho Chi Minh City 701000, Vietnam; Vietnam National University Ho Chi Minh City, Ho Chi Minh City 701000, Vietnam*

Nguyen Tri − *Institute of Chemical Technology−Vietnam Academy of Science and Technology, Ho Chi Minh City 701000, Vietnam;* orcid.org/0000-0001-9486-5096

Nguyen Phung Anh − *Institute of Chemical Technology−Vietnam Academy of Science and Technology, Ho Chi Minh City 701000, Vietnam*

Complete contact information is available at: https://pubs.acs.org/10.1021/acsomega.2c01931

Author Contributions

The authors contributed equally.

Notes

The authors declare no competing financial interest.

https://doi.org/10.1021/acsomega.2c01931
ACS Omega 2022, 7, 20092−20103

■ ACKNOWLEDGMENTS

We acknowledge the support of time and facilities from Ho Chi Minh City University of Technology (HCMUT), VNU-HCM, for this study.

■ ABBREVIATIONS

DRM, dry methane reforming; SRM, steam reforming; BRM, combined steam and CO_2 reforming of CH_4; GHG, greenhouse gases; XRD, X-ray diffraction; H_2-TPR, hydrogen temperature-programmed reduction; SEM, scanning electron microscopy; TEM, transmission electron microscopy; TPO, temperature-programmed oxidation

■ REFERENCES

(1) Habibi, N.; Rezaei, M.; Majidian, N.; Andache, M. CH_4 reforming with CO_2 for syngas production over La_2O_3 promoted Ni catalysts supported on mesoporous nanostructured γ-Al_2O_3. *J. Energy Chem.* **2014**, *23* (4), 435−442.

(2) Therdthianwong, S.; Siangchin, C.; Therdthianwong, A. Improvement of coke resistance of Ni/Al_2O_3 catalyst in CH_4/CO_2 reforming by ZrO_2 addition. *Fuel Process. Technol.* **2008**, *89* (2), 160−168.

(3) Abdullah, B.; Abd Ghani, N. A.; Vo, D.-V. N. Recent advances in dry reforming of methane over Ni-based catalysts. *J. Cleaner Prod.* **2017**, *162*, 170−185.

(4) Han, J. W.; Park, J. S.; Choi, M. S.; Lee, H. Uncoupling the size and support effects of Ni catalysts for dry reforming of methane. *Appl. Catal. B: Environ.* **2017**, *203*, 625−632.

(5) Wang, S.; Lu, G. Catalytic activities and coking characteristics of oxides-supported Ni catalysts for CH_4 reforming with carbon dioxide. *Energy Fuels* **1998**, *12* (2), 248−256.

(6) Wu, P.; Li, X.; Ji, S.; Lang, B.; Habimana, F.; Li, C. Steam reforming of methane to hydrogen over Ni-based metal monolith catalysts. *Catal. Today* **2009**, *146* (1−2), 82−86.

(7) Al-Fatesh, A. S.; Arafat, Y.; Atia, H.; Ibrahim, A. A.; Ha, Q. L. M.; Schneider, M.; M-Pohl, M.; Fakeeha, A. H. CO_2-reforming of methane to produce syngas over Co-Ni/SBA-15 catalyst: effect of support modifiers (Mg, La and Sc) on catalytic stability. *J. CO_2Util.* **2017**, *21*, 395−404.

(8) Shanmugam, V.; Zapf, R.; Neuberg, S.; Hessel, V.; Kolb, G. Effect of ceria and zirconia promotors on Ni/SBA-15 catalysts for coking and sintering resistant steam reforming of propylene glycol in microreactors. *Appl. Catal. B: Environ.* **2017**, *203*, 859−869.

(9) Rodriguez-Gomez, A.; Pereniguez, R.; Caballero, A. Nickel particles selectively confined in the mesoporous channels of SBA-15 yielding a very stable catalyst for DRM reaction. *J. Phys. Chem. B* **2018**, *122* (2), 500−510.

(10) Wang, N.; Chu, W.; Zhang, T.; Zhao, X. Synthesis, characterization and catalytic performances of Ce-SBA-15 supported nickel catalysts for methane dry reforming to hydrogen and syngas. *Int. J. Hydrogen Energy* **2012**, *37* (1), 19−30.

(11) Akri, M.; Zhao, S.; Li, X.; Zang, K.; Lee, A. F.; Isaacs, M. A.; Xi, W.; Gangarajula, Y.; Luo, J.; Ren, Y.; et al. Atomically dispersed nickel as coke-resistant active sites for methane dry reforming. *Nat. Commun.* **2019**, *10* (1), 5181.

(12) Albarazi, A.; Beaunier, P.; Da Costa, P. Hydrogen and syngas production by methane dry reforming on SBA-15 supported nickel catalysts: On the effect of promotion by $Ce_{0.75}Zr_{0.25}O_2$ mixed oxide. *Int. J. Hydrogen Energy* **2013**, *38* (1), 127−139.

(13) Santos, A.; Damyanova, S.; Teixeira, G.; Mattos, L. V.; Noronha, F. B.; Passos, F. B.; Bueno, J. The effect of ceria content on the performance of Pt/CeO_2/Al_2O_3 catalysts in the partial oxidation of methane. *Appl. Catal. A: Gen.* **2005**, *290* (1−2), 123−132.

(14) Nagaraja, B. M.; Bulushev, D. A.; Beloshapkin, S.; Ross, J. R. The effect of potassium on the activity and stability of Ni-MgO-ZrO_2 catalysts for the dry reforming of methane to give synthesis gas. *Catal. Today* **2011**, *178* (1), 132−136.

(15) Zhang, L.; Zhang, Q.; Liu, Y.; Zhang, Y. Dry reforming of methane over Ni/MgO-Al_2O_3 catalysts prepared by two-step hydrothermal method. *Appl. Surf. Sci.* **2016**, *389*, 25−33.

(16) Chong, C. C.; Teh, L. P.; Setiabudi, H. D. Syngas production via CO_2 reforming of CH_4 over Ni-based SBA-15: Promotional effect of promoters (Ce, Mg, and Zr). *Mater. Today Energy* **2019**, *12*, 408−417.

(17) Zhu, J.; Peng, X.; Yao, L.; Tong, D.; Hu, C. CO_2 reforming of methane over Mg-promoted Ni/SiO_2 catalysts: the influence of Mg precursors and impregnation sequences. *Catal. Sci. Technol.* **2012**, *2* (3), 529−537.

(18) Sharifi Pajaie, H.; Taghizadeh, M. Investigation of promoted Cu/ZnO/Al_2O_3 methanol steam reforming nanocatalysts by full factorial design. *Chem. Eng. Technol.* **2012**, *35* (10), 1857−1864.

(19) Roh, H.-S.; Koo, K. Y.; Jeong, J. H.; Seo, Y. T.; Seo, D. J.; Seo, Y.-S.; Yoon, W. L.; Park, S. B. Combined reforming of methane over supported Ni catalysts. *Catal. Lett.* **2007**, *117* (1−2), 85−90.

(20) Loc, L. C.; Phuong, P. H.; Thao, N. H. P.; Tri, N.; Van, N. T. T.; Cuong, H. T.; Anh, H. C. Influence of preparation method on the activity of NiO+MgO/Al_2O_3 catalyst in dry reforming of methane. *Vietnam J. Chem.* **2017**, *55* (3e), 1−7.

(21) Loc, L. C.; Phuong, P. H.; Putthea, D.; Tri, N.; Van, N. T. T.; Cuong, H. T. Effect of CeO_2 morphology on performance of NiO/CeO_2 catalyst in combined steam and CO_2 reforming of CH_4. *Int. J. Nanotechnol.* **2018**, *15* (11−12), 968−982.

(22) Phuong, P. H.; Loc, L. C.; Cuong, H. T.; Tri, N. Effect of NiO loading and thermal treatment duration on performance of Ni/SBA-15 catalyst in combined steam and CO_2 reforming of CH_4. *Mater. Trans.* **2018**, *59* (12), 1898−1902.

(23) Phuong, P. H.; Loc, L. C.; Tri, N.; Anh, N. P.; Anh, H. C. Effect of NH_3 alkalization and MgO promotion on the performance of Ni/SBA-15 catalyst in combined steam and carbon dioxide reforming of methane. *J. Nanomater.* **2021**, *2021*, 1.

(24) Phuong, P. H.; Loc, L. C.; Tri, N.; Van, N. T. T.; Anh, N. P.; Duy, N. P. H.; Cuong, H. T. Effect of V_2O_5 promoter on characteristics and performance of NiO/CeO_2 catalyst in methane bi-reforming. *Adv. Nat. Sci.: Nanosci. Nanotechnol.* **2020**, *11* (4), 045013.

(25) Zhang, H.; Li, M.; Xiao, P.; Liu, D.; Zou, C.-J. Structure and catalytic performance of Mg-SBA-15-supported nickel catalysts for CO_2 reforming of methane to syngas. *Chem. Eng. Technol.* **2013**, *36* (10), 1701−1707.

(26) Păcurariu, C.; Lazău, I.; Ecsedi, Z.; Lazău, R.; Barvinschi, P.; Mărginean, G. New synthesis methods of $MgAl_2O_4$ spinel. *Eur. Ceram. Soc.* **2007**, *27*, 707−710.

(27) Martınez, R.; Romero, E.; Guimon, C.; Bilbao, R. CO_2 reforming of methane over coprecipitated Ni-Al catalysts modified with lanthanum. *Appl. Catal. A: Gen.* **2004**, *274* (1−2), 139−149.

(28) Huang, B.; Li, X.; Ji, S.; Lang, B.; Habimana, F.; Li, C. Effect of MgO promoter on Ni-based SBA-15 catalysts for combined steam and carbon dioxide reforming of methane. *J. Nat. Gas Chem.* **2008**, *17* (3), 225−231.

(29) Spanier, J. E.; Robinson, R. D.; Zhang, F.; Chan, S.-W.; Herman, I. P. Size-dependent properties of CeO_{2-y} nanoparticles as studied by Raman scattering. *Phys. Rev. B* **2001**, *64* (24), 245407.

(30) Perez-Alonso, F.; Melián-Cabrera, I.; Lopez Granados, M.; Kapteijn, F.; Fierro, J. G. Synergy of $Fe_xCe_{1-x}O_2$ mixed oxides for N_2O decomposition. *J. Catal.* **2006**, *239* (2), 340−346.

(31) He, L.; Liang, B.; Li, L.; Yang, X.; Huang, Y.; Wang, A.; Wang, X.; Zhang, T. Cerium-oxide-modified nickel as a non-noble metal catalyst for selective decomposition of hydrous hydrazine to hydrogen. *ACS Catal.* **2015**, *5* (3), 1623−1628.

(32) Laguna, O.; Centeno, M.; Boutonnet, M.; Odriozola, J. A. Fe-doped ceria solids synthesized by the microemulsion method for CO oxidation reactions. *Appl. Catal. B: Environ.* **2011**, *106* (3−4), 621−629.

(33) Stoian, D.; Medina, F.; Urakawa, A. Improving the stability of CeO_2 catalyst by rare earth metal promotion and molecular insights in

https://doi.org/10.1021/acsomega.2c01931
ACS Omega 2022, 7, 20092−20103

the dimethyl carbonate synthesis from CO_2 and methanol with 2-cyanopyridine. *ACS Catal.* **2018**, *8* (4), 3181−3193.
(34) Kim, J.-H.; Suh, D. J.; Park, T.-J.; Kim, K.-L. Effect of metal particle size on coking during CO_2 reforming of CH_4 over Ni-alumina aerogel catalysts. *Appl. Catal. A: Gen.* **2000**, *197* (2), 191−200.
(35) Van, N. T.; Loc, L. C.; Anh, N. P.; Cuong, H. T.; Tri, N. Positive effects of CeO_2 promoter and co-reactant/CO on methanation of CO_2-rich gas over Ni/SBA-15 catalyst. *Mater. Trans.* **2020**, *61* (7), 1332−1338.
(36) Song, Z.; Liu, W.; Nishiguchi, H. Quantitative analyses of oxygen release/storage and CO_2 adsorption on ceria and Pt-Rh/ceria. *Catal. Commun.* **2007**, *8* (4), 725−730.
(37) Hojo, H.; Mizoguchi, T.; Ohta, H.; Findlay, S. D.; Shibata, N.; Yamamoto, T.; Ikuhara, Y. Atomic structure of a CeO_2 grain boundary: the role of oxygen vacancies. *Nano Lett.* **2010**, *10* (11), 4668−4672.
(38) Vivier, L.; Duprez, D. Ceria-based solid catalysts for organic chemistry. *ChemSusChem* **2010**, *3* (6), 654−678.
(39) Xu, B.; Zhang, Q.; Yuan, S.; Zhang, M.; Ohno, T. Morphology control and characterization of broom-like porous CeO_2. *Chem. Eng. J.* **2015**, *260*, 126−132.
(40) Cui, Z.; Gan, J.; Fan, J.; Xue, Y.; Zhang, R. Size-dependent surface basicity of nano-CeO_2 and desorption kinetics of CO_2 on its surface. *Ind. Eng. Chem. Res.* **2018**, *57* (32), 10977−10984.
(41) Pakhare, D.; Shaw, C.; Haynes, D.; Shekhawat, D.; Spivey, J. Effect of reaction temperature on activity of Pt-and Ru-substituted lanthanum zirconate pyrochlores ($La_2Zr_2O_7$) for dry (CO_2) reforming of methane (DRM). *J. CO_2Util.* **2013**, *1*, 37−42.
(42) Corthals, S.; Van Nederkassel, J.; Geboers, J.; De Winne, H.; Van Noyen, J.; Moens, B.; Sels, B.; Jacobs, P. Influence of composition of $MgAl_2O_4$ supported $NiCeO_2ZrO_2$ catalysts on coke formation and catalyst stability for dry reforming of methane. *Catal. Today* **2008**, *138* (1−2), 28−32.
(43) Trimm, D. L. Catalysts for the control of coking during steam reforming. *Catal. Today* **1999**, *49* (1−3), 3−10.
(44) Yang, K.; Zhang, Y.; Li, Y.; Huang, P.; Chen, X.; Dai, W.; Fu, X. Insight into the function of alkaline earth metal oxides as electron promoters for Au/TiO_2 catalysts used in CO oxidation. *Appl. Catal. B: Environ.* **2016**, *183*, 206−215.
(45) Zecchina, A.; Coluccia, S.; Spoto, G.; Scarano, D.; Marchese, L. Revisiting MgO-CO surface chemistry: an IR investigation. *J. Chem. Soc., Faraday Trans.* **1990**, *86* (4), 703−709.
(46) Li, K. Z.; Wang, H.; Wei, Y. G.; Yan, D. X. Selective oxidation of carbon using iron-modified cerium oxide. *J. Phys. Chem. C* **2009**, *113* (34), 15288−15297.
(47) Schmitt, R.; Nenning, A.; Kraynis, O.; Korobko, R.; Frenkel, A. I.; Lubomirsky, I.; Haile, S. M.; Rupp, J. L. A review of defect structure and chemistry in ceria and its solid solutions. *Chem. Soc. Rev.* **2020**, *49* (2), 554−592.
(48) Luo, C.; Dou, B.; Zhang, H.; Liu, D.; Zhao, L.; Chen, H.; Xu, Y. Co-production of hydrogen and syngas from chemical looping water splitting coupled with decomposition of glycerol using Fe-Ce-Ni based oxygen carriers. *Energy Convers. Manage.* **2021**, *238*, 114166.
(49) Sai Prasad, P. S.; Bae, J. W.; Jun, K.-W.; Lee, K.-W. Fischer−Tropsch synthesis by carbon dioxide hydrogenation on Fe-based catalysts. *Catal. Surv. Asia* **2008**, *12* (3), 170−183.
(50) Wu, K.; Dou, B.; Zhang, H.; Liu, D.; Chen, H.; Xu, Y. Aqueous phase reforming of biodiesel byproduct glycerol over mesoporous Ni-Cu/CeO_2 for renewable hydrogen production. *Fuel* **2022**, *308*, 122014.
(51) Dou, B.; Zhao, L.; Zhang, H.; Wu, K.; Zhang, H. Renewable hydrogen production from chemical looping steam reforming of biodiesel byproduct glycerol by mesoporous oxygen carriers. *Chem. Eng. J.* **2021**, *416*, 127612.
(52) Qian, J. X.; Chen, T. W.; Enakonda, L. R.; Liu, D. B.; Mignani, G.; Basset, J.-M.; Zhou, L. Methane decomposition to produce CO_x-free hydrogen and nano-carbon over metal catalysts: A review. *Int. J. Hydrogen Energy* **2020**, *45* (15), 7981−8001.
(53) Luo, J.; Yu, Z.; Ng, C.; Au, C. CO_2/CH_4 reforming over Ni-La_2O_3/5A: an investigation on carbon deposition and reaction steps. *J. Catal.* **2000**, *194* (2), 198−210.
(54) Liu, C. j.; Ye, J.; Jiang, J.; Pan, Y. Progresses in the preparation of coke resistant Ni-based catalyst for steam and CO_2 reforming of methane. *ChemCatChem.* **2011**, *3* (3), 529−541.
(55) Wang, S.; Lu, G.; Millar, G. J. Carbon dioxide reforming of methane to produce synthesis gas over metal-supported catalysts: state of the art. *Energy Fuels* **1996**, *10* (4), 896−904.
(56) Olah, G. A.; Goeppert, A.; Czaun, M.; Mathew, T.; May, R. B.; Prakash, G. S. Single step bi-reforming and oxidative bi-reforming of methane (natural gas) with steam and carbon dioxide to metgas (CO-$2H_2$) for methanol synthesis: self-sufficient effective and exclusive oxygenation of methane to methanol with oxygen. *J. Am. Chem. Soc.* **2015**, *137* (27), 8720−8729.
(57) Sharma, S.; Hilaire, S.; Vohs, J.; Gorte, R.; Jen, H.-W. Evidence for oxidation of ceria by CO_2. *J. Catal.* **2000**, *190* (1), 199−204.
(58) Chen, Q.; Lua, A. C. Synthesis of electroless Ni catalyst supported on SBA-15 for hydrogen and carbon production by catalytic decomposition of methane. *Int. J. Energy Res.* **2021**, *45* (2), 2810−2823.
(59) Hou, Z.; Yashima, T. Meso-porous Ni/Mg/Al catalysts for methane reforming with CO_2. *Appl. Catal. A: Gen* **2004**, *261* (2), 205−209.
(60) Das, S.; Sengupta, M.; Patel, J.; Bordoloi, A. A study of the synergy between support surface properties and catalyst deactivation for CO_2 reforming over supported Ni nanoparticles. *Appl. Catal. A: Gen.* **2017**, *545*, 113−126.
(61) Zhang, J.; Li, F. Coke-resistant Ni@SiO_2 catalyst for dry reforming of methane. *Appl. Catal. B: Environ.* **2015**, *176*, 513−521.
(62) Konigsberger, E.; Konigsberger, L.-C.; Gamsjager, H. Low-temperature thermodynamic model for the system Na_2CO_3-$MgCO_3$-$CaCO_3$-H_2O. *Geochim. Cosmochim. Acta* **1999**, *63* (19−20), 3105−3119.
(63) Roh, H.-S.; Jun, K.-W.; Park, S.-E. Methane-reforming reactions over Ni/Ce-ZrO_2/θ-Al_2O_3 catalysts. *Appl. Catal. A: Gen.* **2003**, *251* (2), 275−283.
(64) Giordano, F.; Trovarelli, A.; de Leitenburg, C.; Giona, M. A model for the temperature-programmed reduction of low and high surface area ceria. *J. Catal.* **2000**, *193* (2), 273−282.
(65) Shan, W.; Luo, M.; Ying, P.; Shen, W.; Li, C. Reduction property and catalytic activity of $Ce_{1-X}Ni_XO_2$ mixed oxide catalysts for CH_4 oxidation. *Appl. Catal. A: Gen.* **2003**, *246* (1), 1−9.
(66) Trovarelli, A.; de Leitenburg, C.; Dolcetti, G. Design better cerium-based oxidation catalysts. *Chemtech* **1997**, *27* (6), 32−37.
(67) Li, H.; Ren, J.; Qin, X.; Qin, Z.; Lin, J.; Li, Z. Ni/SBA-15 catalysts for CO methanation: effects of V, Ce, and Zr promoters. *RSC Adv.* **2015**, *5* (117), 96504−96517.
(68) Aziz, M.; Jalil, A.; Triwahyono, S.; Saad, M. CO_2 methanation over Ni-promoted mesostructured silica nanoparticles: Influence of Ni loading and water vapor on activity and response surface methodology studies. *Chem. Eng. J.* **2015**, *260*, 757−764.
(69) Hu, Y. H.; Ruckenstein, E. Binary MgO-based solid solution catalysts for methane conversion to syngas. *Catal. Rev.* **2002**, *44* (3), 423−453.
(70) Kuzmin, A.; Mironova, N. Composition dependence of the lattice parameter in solid solutions. *J. Phys.: Condens. Matter* **1998**, *10* (36), 7937.
(71) Wang, H.; Ruckenstein, E. CO_2 reforming of CH_4 over Co/MgO solid solution catalysts - effect of calcination temperature and Co loading. *Appl. Catal. A: Gen.* **2001**, *209* (1−2), 207−215.
(72) Yan, Y.; Dai, Y.; He, H.; Yu, Y.; Yang, Y. A novel W-doped Ni-Mg mixed oxide catalyst for CO_2 methanation. *Appl. Catal. B: Environ.* **2016**, *196*, 108−116.
(73) Kasza, R.; Griffiths, K.; Shapter, J.; Norton, P.; Harrington, D. Interaction of water with stepped Ni (760): associative versus dissociative adsorption and autocatalytic decomposition. *Surf. Sci.* **1996**, *356* (1−3), 195−208.

https://doi.org/10.1021/acsomega.2c01931
ACS Omega 2022, 7, 20092−20103